Superlattices and Microstructures 140 (2020) 106449

Contents lists available at ScienceDirect

Superlattices and Microstructures

journal homepage: www.elsevier.com/locate/superlattices

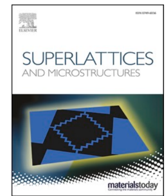

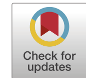

Transport and magnetic phenomena in ZnO-C thin-film heterostructures

M.N. Volochaev [a], A.B. Granovsky [b], O.V. Zhilova [c], Yu.E. Kalinin [c], V.V. Ryl'kov [d], M. P. Sumets [e,*], V.A. Makagonov [c], S. Yu Pankov [c], A.V. Sitnikov [c], E. Fadeev [f], E. Lahderanta [f], V.A. Foshin [c]

[a] Kirensky Institute of Physics, Krasnoyarsk, 660036, Russia
[b] Lomonosov Moscow State University, Moscow, 119991, Russia
[c] Voronezh State Technical University, Voronezh, 394026, Russia
[d] National Research Centre "Kurchatov Institute", Moscow, 123182, Russia
[e] Voronezh State University, Voronezh, 394003, Russia
[f] Lappeenranta-Lahti University of Technology, Lappeenranta FI, 53851, Finland

A R T I C L E I N F O

Keywords:
Zinc oxide
Amorphous carbon
Multi-layered structures
Composites
Hopping conductivity
Weak localization
Magnetoresistance

A B S T R A C T

ZnO- and C-based heterostructures were fabricated by the layer-by-layer deposition technique using the ion-beam sputtering process. Structure, electrical and magnetic properties of fabricated heterostructures are discussed. The two-phase (ZnO and C) films are evolved into a multilayer structure, consisting of amorphous carbon and crystalline ZnO layers when the bilayer thickness increases. When carbon is added to ZnO, its electrical resistivity reduces. The conduction mechanism changes from the variable-range hopping in a narrow energy band to the nearest neighbors hopping in ZnO–C films with a thickness of $h < 150$ nm. The temperature dependence of conductivity changes from the Arrhenius-like to logarithmic law, indicating that the strong charge localization turns into a weak one when the film thickness is about 150 nm. The negative magnetoresistance of up to 1%was detected at 77 K. The film ferromagnetism at the temperature of 10 K was not found.

1. Introduction

The diluted magnetic semiconductors (DMS) are great of interest due to a wide range of their applications like spintronics which base on spin-dependent transport [1,2]. Primarily, DMS are fabricated through the doping of semiconductors by transition metals (TM). As predicted, ZnO and GaN are the ideal candidates for DMS at room temperatures [1]. Even though that ferromagnetism is observed in ZnO-based systems, doped by TM and even without doping in dielectric oxides [3], the reported experimental results are controversial and the origin of ferromagnetism is not clear. Hypothetically, the TM doping produces clusters of the secondary phases, making properties of DMS worse. Thus, the new alternative doping elements like carbon have been investigated actively. Many researchers reported that ZnO, doped by non-magnetic C, manifests the room-temperature ferromagnetism (RTFM) [4,5]. Nevertheless, the physical nature of this phenomenon is still discussing.

Nowadays, there are two explanations of RTFM in the ZnO–C system. The first explanation implies that the hole-mediated exchange

* Corresponding author.
E-mail address: maxsumets@gmail.com (M.P. Sumets).

https://doi.org/10.1016/j.spmi.2020.106449
Received 11 November 2019; Received in revised form 5 February 2020; Accepted 17 February 2020
Available online 21 February 2020
0749-6036/© 2020 Elsevier Ltd. All rights reserved.

interaction exist in ZnO:C. This interaction occurs between 2p-localized spins of C atoms, residing in O- atomic positions of ZnO (p-p exchange interaction). This model postulates that ZnO:C is a p-type semiconductor contrary to the theoretical models predicting an n-type conductivity of C-doped ZnO films, and manifesting the RTFM [6,7]. Besides, the majority of carbon atoms are in the intersite or Zn positions or forming the graphite-like clusters [5,8]. Thus, the role of carbon in the ferromagnetic ordering of ZnO is still unclear.

The second approach is based on the defect-induced ferromagnetism [1,2]. The ferromagnetic ordering (d^0 -ferromagnetism) as a common effect, supporting this model and originated from RTFM, was detected in pure undoped oxides such as TiO_2, In_2O_3, SnO_2, Cu_2O и MgO [9–13]. According to the density functional theory (DFT), ferromagnetism in ZnO does not stem from the non-paired 2p-states of O atoms neighboring the zinc vacancies (V_{Zn}) and causing the spin polarization in the valence band (V_B) [14]. The strong exchange interaction between 2p orbitals O and high effective masses of carriers near the top of V_B satisfy the Stoner criteria for the occurrence of spontaneous ferromagnetism. This effect cannot be attained easily by doping with the acceptor impurities residing in the O sites in ZnO [15,16]. As emphasized in the works [17–19], oxygen vacancies (V_O) or intersite Zn atoms in the ZnO low-dimension systems like thin films, nanoparticles, and nanowires can trigger the RTFM. Thus, it is still unclear what role the oxygen and zinc vacancies, as well as surface defects, play in the occurrence of d^0-ferromagnetism. Besides, the grain boundaries and interfaces affect the charge transport in oxide semiconductors greatly [20]. The most prominentlythis effect is observed in thin films where the film-substrate interface and film surface influence the charge transport. Consequently, the magnetic properties and transport phenomena in the doped ZnO are interdependent.

From this point of view, the nanostructured ZnO with various types of Zn/O interfaces (ordered and disordered) poses an interest in the study of magnetic ordering and electrical properties of the Zn–O system. It is undoubtedly true that the fabrication technique and conditions dictate the structure and properties of thin films.

Being an effective deposition technique, an ion-beam sputtering method has not utilized for the fabrication of single- and multi-layered ZnO-C heterostructures. Taking into account that the film structure and properties depend on the fabrication method greatly, this paper aims to investigate the structure, charge transport and magnetic properties of ZnO- and C-based multilayer systems, fabricated by the ion-beam sputtering method.

2. Materials and method

Multilayer ZnO–C thin films were fabricated by layer-by-layer ion-beam sputtering of the ZnO and C ceramic targets in an argon atmosphere with a purity of 99.998% at a pressure of 7×10^{-4} Torr as described in Ref. [21]. The targets were fixed and differently positioned in a vacuum chamber on the water-cooled 280×80 mm^2 copper bases. The substrates were located offset from the target erosion zone during the ion-beam sputtering to eliminate the plasma effect on a growing film. A massive aluminum bar served as a substrate holder getting off heat released under the film growth process. The surface temperature was controlled by five thermocouples positioned uniformly along the surface. During the deposition lasting for 3 h 12min and 5 h 50min for the $(ZnO/C)_{25}$ and $(ZnO/C)_{81}$ films respectively, the temperature did not deviate from room temperature more than by 2°. To carry out the layer-by-layer deposition at room temperature, the substrates were moved from one sputtering position to another one, by rotating the substrate holder around a sputtering chamber axis. The silicon wafers (100)Si and pyroceramics were used to investigate the structure and electrical properties respectively. A V-shaped screen was installed between the target and the substrate holder to vary the C- interlayer thickness during a single deposition process. The rotational speed was equal to 0.13 rpm and 0.23 rpm for $(ZnO/C)_{25}$ and $(ZnO/C)_{81}$ films respectively. The numbers 25 and 81 mean the number of passes through the deposition stages, where ZnO and C were sequentially deposited onto a substrate. As demonstrated further, the rotation speed is critical to the film structure. In total 150 samples were fabricated.

To estimate the thickness of each layer in a multilayer structure, a preliminary deposition of single-phase ZnO and C films was performed with the pre-selected process parameters. The thickness of the obtained films was measured using the optical interferometer (MII-4). Knowing the number of revolutions of a carousel, it is possible to calculate the thickness of a monolayer-film, deposited when the substrate passes once the area of material deposition. It is worth noting, that the monolayer thickness estimated by this method, does not account for the possible island growth (i.e. this is the effective thickness provided that this film is continuous).

The number of the substrate holder revolutions determines the number of bilayers in a multilayer heterostructure. According to the method described above, 25 and 81 equivalent bilayers were deposited for each sample at the rotational speed of 0.13 rpm and 0.23 rpm respectively. The total thickness of the multilayers ranged from 40 to 160 nm.

The study of elemental composition was conducted using scanning electron microscopy (SEM, Oxford INCA Energy 250 with an energy dispersive X-ray add-on device on a JEOL JSM-6380 L V). The structure was investigated by X-ray diffraction methods (XRD, Bruker D2 Phaser diffractometer, $\lambda_{CuK\alpha1} = 1.54$ Å) with the DIFFRAC.EVA 3.0 software and the ICDD PDF Release 2012 database. The transmission electron microscopy (TEM) patterns were obtained by a Hitachi HT7700 microscope with an accelerating voltage of 100 kV (W source). The cross-sections of about 40–50 nm thick were made using a single-beam system (a focused ion beam system FIB, Hitachi FB2100). The electrical resistivity of the studied films was measured by the two-probe method using a B7-78/1 universal digital multimeter with errors not exceeding 2%. The thermopower was investigated by the differential method with errors not exceeding 3%. Silver (99.99% of purity) was used as a material for the cold and hot probes.

The Hall measurements were conducted by the Van der Pauw method (ECOPIA HMS-5500) at room temperature and the magnetic field of 0.55 T with the measuring current ranged from 0.1 to 2.0 mA.

The field dependence of magnetization was measured using a SQUID magnetometer (Cryogenic S700X) in the range of ±5 T at a temperature of 10 K. The samples were located vertically in the magnetometer, with their long axis oriented to the field.

3. Results and discussion

The analysis of XRD spectra (Fig. 1a) of thin films deposited onto a rotating substrate revealed that thin carbon films are amorphous [22], whereas a single-phase ZnO sample has the hexagonal crystal structure with the P63mc space group [23]. The multilayer films $(ZnO/C)_{81}$ manifest a texture with the <001>axis perpendicular to the substrate.

The small-angle XRD pattern of the $(ZnO/C)_{81}$ system (Fig. 2a) does not manifest any diffraction maxima, suggesting that an island structure, rather than a multilayer film, is formed in each layer. Consequently, it can be assumed that the zinc oxide nanocrystallites and the amorphous carbon phase are coexisted in $(ZnO/C)_{81}$ films. Thus, despite the layer-by-layer deposition of ZnO and C, the $(ZnO/C)_{81}$ system is a composite with the blurred interlayer interfaces. Therefore, the total film thickness, rather than an equivalent bilayer thickness, has to be used to describe these samples.

As follows from the XRD patterns (Fig. 1b), the $(ZnO/C)_{25}$ system contains the ZnO crystalline phase. The small-angle XRD patterns (Fig. 2b) contain the diffraction peaks, attributed to the formation of a layered structure. The period of the multilayer structure *d* was calculated through the Bragg formula:

$$n\lambda = 2d \sin \theta \tag{1}$$

here, θ is the Bragg angle, n is the diffraction maximum order (in our case $n = 1$), and λ is the X-ray wavelength.

The obtained values of d for the $(ZnO/C)_{25}$ multilayer heterostructures are in good agreement with those obtained through the optical interferometry.

Fig. 3 shows the TEM micrographs of the studied $(ZnO/C)_{81}$ and $(ZnO/C)_{25}$ films, demonstrating the nanocrystalline structure of the studied samples. Besides, the electron diffraction patterns (see insets in Fig. 3a and b) reveal the phases of hexagonal crystalline ZnO. As mentioned above, analyzing the small-angle XRD patterns, the layered structure is formed for all thin $(ZnO/C)_{25}$ films (Fig. 3b), whereas the $(ZnO/C)_{81}$ system is a randomly distributed composite (Fig. 3a).

Fig. 4a shows the electrical resistivity as a function of thickness for the studied ZnO and $(ZnO/C)_{81}$ samples. As seen from Fig. 4, the electrical resistivity of thin $(ZnO/C)_{81}$ films two orders of magnitude lower than that for a pure ZnO. The reason is that $(ZnO/C)_{81}$ films have a higher number of interfaces and grain boundaries (being the charge transport channels in wide-gap semiconductors [24]) compared to ZnO. The sign of thermopower (Fig. 4b) indicates that both $(ZnO/C)_{81}$ and ZnO films are the n-type semiconductors.

The electrical resistivity and thermopower of $(ZnO/C)_{81}$ layered structure decrease from $1.7\cdot10^{-2}$ Ω cm to $4.9\cdot10^{-3}$ Ω cm and from 65 μV/K to 47 μV/K when the film thickness rises from 30 nm to 130 nm respectively.

As regards the $(ZnO/C)_{25}$ multilayer structure, it demonstrates a threefold decrease in the electrical resistivity with the thickness

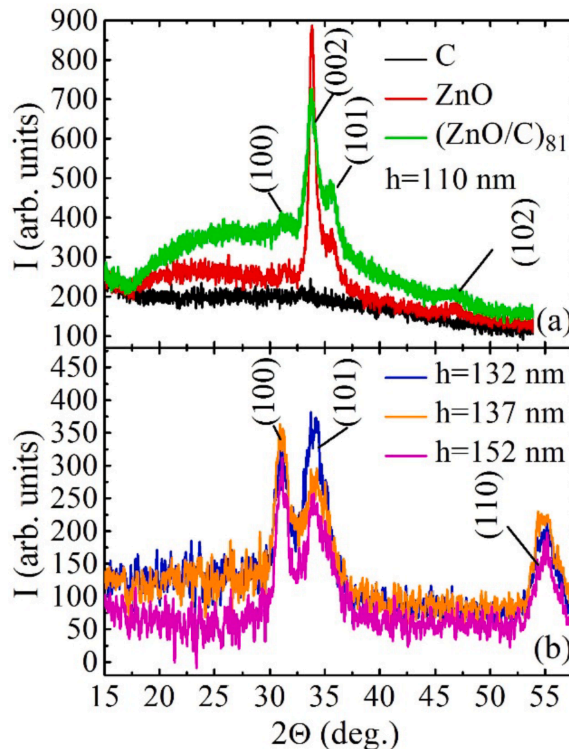

Fig. 1. XRD patterns of C, ZnO, and $(ZnO/C)_{81}$ thin films with the thickness of $h = 110$ nm (a) and $(ZnO/C)_{25}$ (b) with the thickness of 132 nm, 137 nm, and 152 nm.

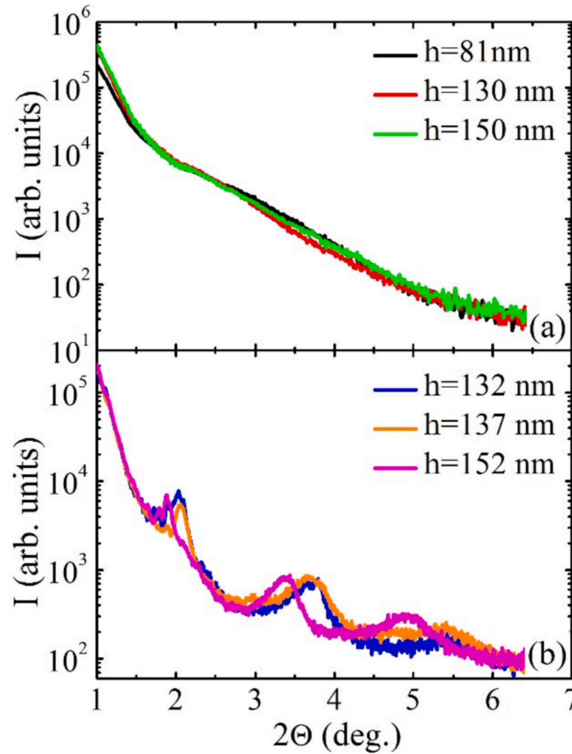

Fig. 2. Small-angle XRD pattern of $(ZnO/C)_{81}$ (a) and $(ZnO/C)_{25}$ (b) thin films.

(see Fig. 5a). The negative sign of thermopower indicates that electrons are the major charge carriers (Fig. 5b). The electrical resistivity of $(ZnO/C)_{25}$ increases with the amount of ZnO in it.

The Hall measurements at room temperature also confirm that the addition of carbon in ZnO does not change its conductivity type. The charge carrier concentration is a weak linear function of the film thickness for $(ZnO/C)_{81}$ and decreases from $5{\cdot}10^{20}$ to $8{\cdot}10^{20}$ cm^{-3} when the thickness rises from 30 nm to 130 nm respectively. Fig. 6 demonstrates how the charge mobility μ depends on the film thickness. A broad maximum with the magnitude of 2 $cm^2\,V^{-1}\,s^{-1}$, corresponding to the thickness of ~80 nm, is observed on the $\mu(h)$ curve shown in Fig. 6. An increase in the carrier mobility with the thickness d up to 80 nm can be attributed to the classical size effect at the thin film boundaries. The μ declines with $h > 80$ nm, due to the scattering processes at the ZnO/C interfaces.

For the $(ZnO/C)_{25}$ films the carrier concentration and mobility decrease from $3.2{\cdot}10^{20}$ cm^{-3} to $1.6{\cdot}10^{20}$ cm^{-3} and from 1.4 $cm^2V^{-1}{\cdot}s^{-1}$ to 2.8 $cm^2V^{-1}{\cdot}s^{-1}$ respectively when the film thickness rises from 130 nm to 155 nm. The “apparent” decrease in mobility occurs due to electronic states existing at the layer interfaces in the $(ZnO/C)_{25}$ films and influencing the charge transport. When the thickness and number of ZnO and C layers increase their structure remains the same. Consequently, the number of carriers taking part in the charge transport does not change when the amount of material not contributing to the conductivity rises. As a result, the “apparent” decrease in charge concentration occurs. An increase in mobility of the $(ZnO/C)_{25}$ films stems from the classical size effect at the boundaries.

The temperature dependence of electrical resistivity ρ(T) was studied at the temperatures ranged from 80 to 300 K (Fig. 7), to determine the charge transport mechanisms in the samples $(ZnO/C)_{81}$ and $(ZnO/C)_{25}$. As seen from Fig. 7, the electrical resistivity decreases with temperature over the entire temperatures range.

The magnetoresistance (MR) as a function of the magnetic field strength for as-grown layered $(ZnO/C)_{25}$ heterostructures are shown in Fig. 8. The magnitude of MR was determined as $MR = (R_H - R_0)/R_0$, where R_H and R_0 are the resistance, measured in an external magnetic field and without a magnetic field respectively. It follows from Fig. 8 that the electrical resistance declines with the magnetic field strength. For the $(ZnO/C)_{81}$ heterostructures, no change in the electrical resistance was detected under an applied magnetic field of up to 1 T.

The magnetization measurements (see Fig. 9) did not reveal the ferromagnetic ordering at the temperature of 10 K since no hysteresis was detected. This fact rules out the presence of the room temperature magnetism in the studied samples.

Let us discuss the obtained data taking into account the growth process of layered thin-film heterostructures on a rotating substrate with ion-beam sputtering of ZnO and C targets. The $(ZnO/C)_{81}$ system manifests the island-like structure. The electrical resistivity of this two-phase ZnO/C system is much lower than that for ZnO due to the interfaces (Fig. 4a). For the $(ZnO/C)_{25}$ system with the thickness of $h < 140$ nm, the ZnO layers alternate with the carbon island interlayers, decreasing the electrical resistivity (Fig. 5a). When the islands grow in size in the carbon interlayer, they overlap, increasing the dangling bond concentration at the interfaces, and reducing the electrical resistivity of the film (Fig. 5a). Besides, randomly distributed charges generate a chaotic potential. Thus, in this

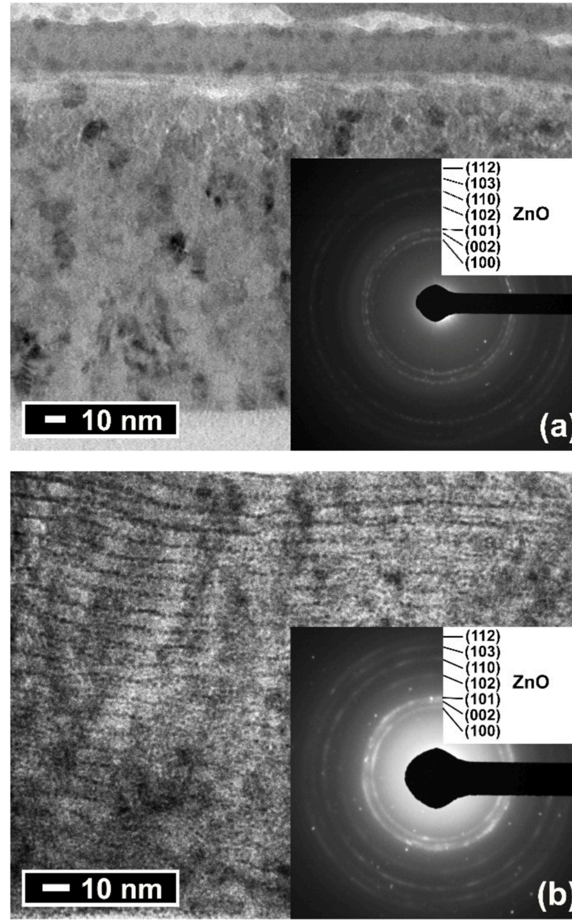

Fig. 3. TEM micrographs of the cross-section and electron diffraction patterns (shown in the insets) for the studied $(ZnO/C)_{81}$ (h_{Bl} = 1.9 nm) (a) and $(ZnO/C)_{25}$ (h_{Bl} = 6.7 nm) (b) heterostructures with the total thickness of h = 157 nm and h = 135 nm respectively.

multilayer system, the strong localization conditions take place at the interfaces with the presence of carbon islands [24].

A layered structure, consisting of ZnO and amorphous carbon layers, is formed in the $(ZnO/C)_{25}$ films more than 150 nm thick. The carbon layers and their interfaces serve as the conductive channels in this type of heterostructures. A transition from the strong to weak localization [25,26] occurs when the thickness of $(ZnO/C)_{25}$ films rises. This transition changes the conduction mechanism. A similar relationship was observed in the multilayer structure $(SnO_2/In_2O_3)_{69}$ [27].

To determine the charge transport mechanisms, we investigated the temperature dependence of resistivity in the studied samples. Figs. 10–12 show the relative resistivity of $(ZnO/C)_{81}$ and $(ZnO/C)_{25}$ films as a function of temperature in various coordinates in the temperature range of 77–170 K.

As seen from Fig. 10, the electrical resistivity is linear in the $\ln(\rho/\rho_0)$-$1/T^{1/3}$ coordinates, which is attributed to the variable range hopping mechanism over the localized states in a narrow energy band near the Fermi level [28]. In the framework of this mechanism, the electrical resistivity is described as follows:

$$\rho = \rho_0 \exp\left(B / T^{1/3}\right) \tag{2}$$

where

$$B = \left[\frac{3}{a^2 k_B g(E_F)}\right]^{1/3} \tag{3}$$

here T is the absolute temperature, $g(E_F)$ is the density of states at the Fermi level, a is the localization radius, and k_B is the Boltzmann constant.

The B magnitudes in (2), obtained from the slope of $\ln(\rho/\rho_0)$-$1/T^{1/3}$ linear graphs (see Fig. 10) are given in Table 1. Accepting a~0.8 Å [29] as the ionic radius of Zn, we estimated the density of states $g(E_F)$ through equation (3) (see Table 1). The obtained results show a high density of localized states at the Fermi level.

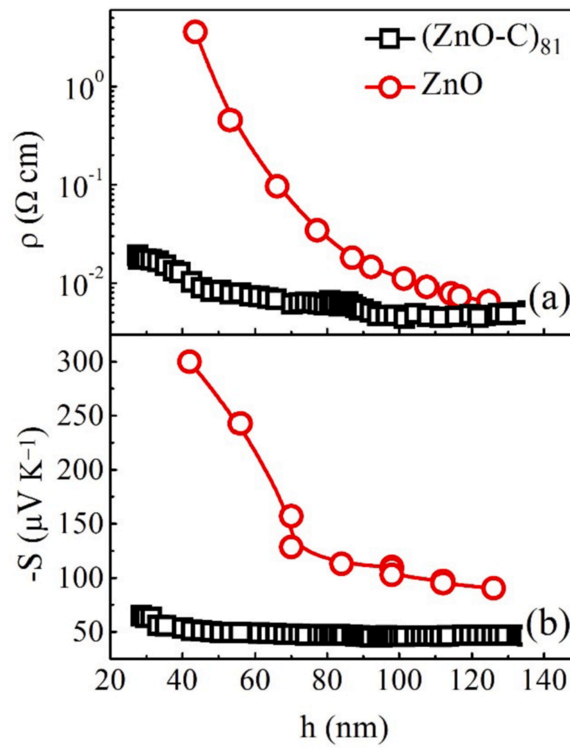

Fig. 4. The electrical resistivity (a) and thermopower (b) as a function of the thickness of thin ZnO and $(ZnO/C)_{81}$ films, measured at room temperature.

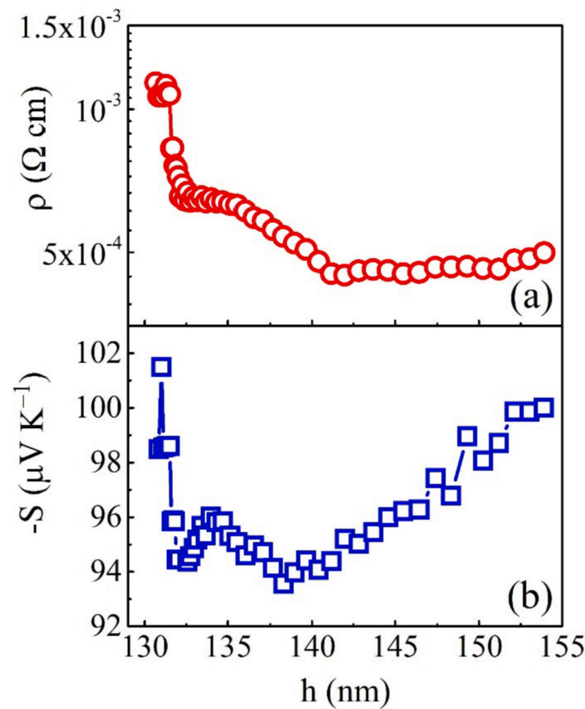

Fig. 5. The electrical resistivity (a) and thermopower (b) as a function of the thickness of thin $(ZnO/C)_{25}$ films, measured at room temperature.

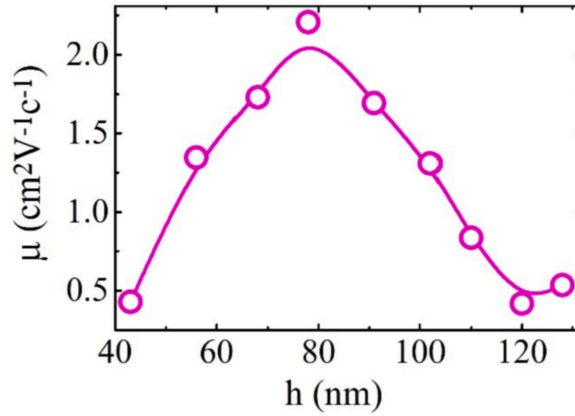

Fig. 6. The carrier mobility as a function of $(ZnO/C)_{81}$ film thickness.

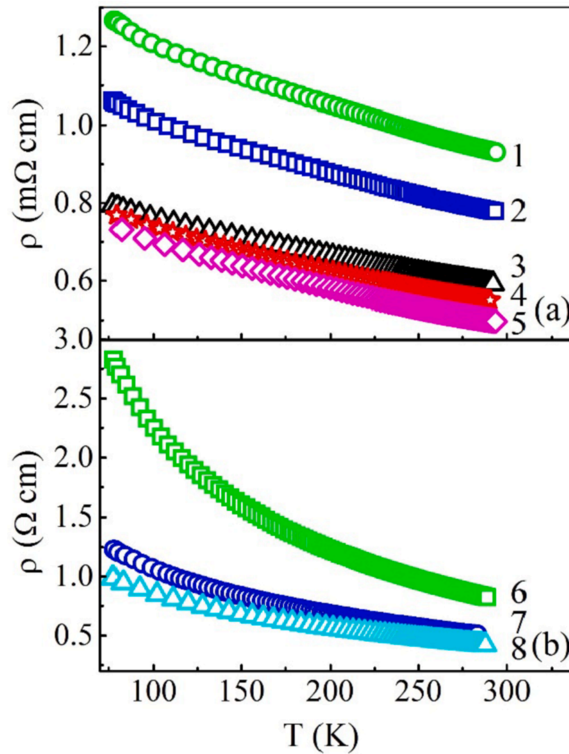

Fig. 7. Temperature dependences of resistivity for thin $(ZnO/C)_{81}$ films (a) and $(ZnO/C)_{25}$ films (b) for various film thicknesses: 1–35 nm, 2–45 nm, 3–70 nm, 4–98 nm, 5–129 nm, 6–150 nm, 7–157 nm, 8–169 nm.

In the temperature range of 200–300 K, the hopping conductivity to the nearest neighbors takes place for the studied samples. According to this mechanism, the temperature dependence of resistivity is given by the following expression [28]:

$$\rho = \rho_0 \cdot \exp\left(- \frac{W_{NNH}}{kT} \right) \tag{4}$$

here W_{NNH} is the hoping activation energy.

The Arrhenius-like temperature dependence of resistivity for the studied $(ZnO/C)_{81}$ films is linear in the $\ln(\rho/\rho_0)$-$1/T$ coordinates in a total agreement with (4) (see Fig. 11). The activation hopping energy estimated from the slope of $\ln(\rho/\rho_0)$-$1/T$ graphs is given in Table 2.

For the $(ZnO/C)_{25}$ multilayer samples with the thickness of $h > 150$ nm (when a continuous carbon layer is formed), the temperature dependence of resistivity is linear in the ρ-$\ln T$ coordinates (see Fig. 12). This dependence is typical when the weak electron

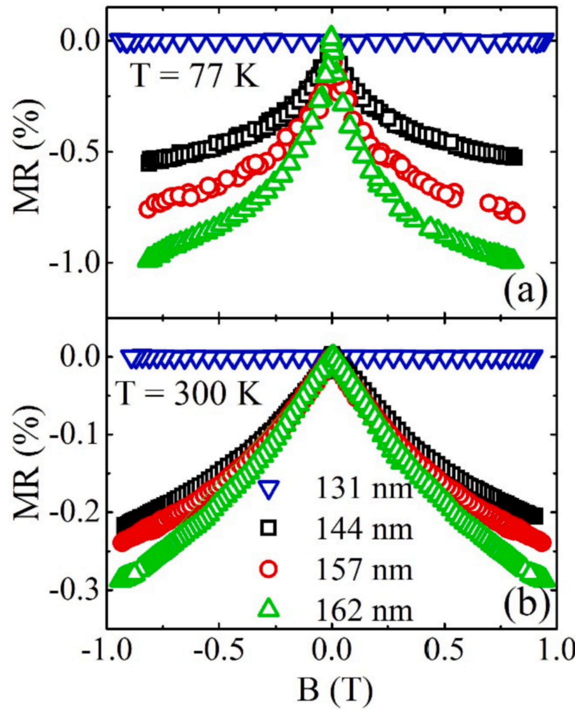

Fig. 8. The electrical resistivity as a function of the magnetic field strength for the $(ZnO/C)_{25}$ and $(ZnO/C)_{81}$ multilayer structures with different bilayer thickness measured at $T = 77$ K (a) and $T = 300$ K (b). (The thickness of $(ZnO/C)_{81}$ multilayer structure is $h = 131$ nm).

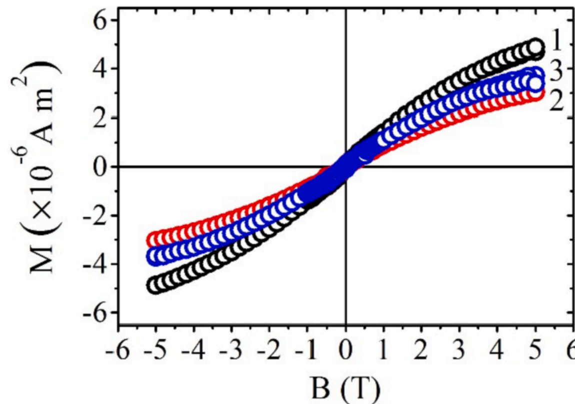

Fig. 9. The magnetization as a function of the magnetic field for multilayer $(ZnO/C)_{25}$ structures with various bilayer thickness: 1–132 nm, 2–136 nm, 3–145 nm and measured at T = 10 K.

localization occurs in 2D and 3D systems [26].

The temperature dependence of resistivity for ZnO:Ga films with a thickness of 100–400 nm, fabricated by the radio-frequency magnetron sputtering process, was studied in the work [30] in the temperature range of 300–80 K. The film resistivity with a thickness of 200 nm declined, whereas for the films 400 nm thick the temperature dependence of resistivity peaked at 160 K.

The observed temperature dependence was explained by the weak charge localization. Besides, the weak localization effects in "thick" films (400 nm) were observed for the temperatures below 160 K. This phenomenon was explained by the low lattice distortions in thick films. Consequently, at the temperature of 160 K, the diffusion length becomes comparable with the free path length within the relaxation time. Also, it was revealed that in ZnO:Ga films, synthesized by the pulsed laser deposition technique, the interference effects in the temperature dependence of resistivity occur at the higher temperatures when the Ga concentration rises. This effect was explained in the work [31] by a defect concentration increase. Taking into account these results the temperature dependence of resistivity observed in our $(ZnO/C)_{25}$ multilayered structures with a thickness of 150 nm at low temperatures can be associated with the weak charge localization.

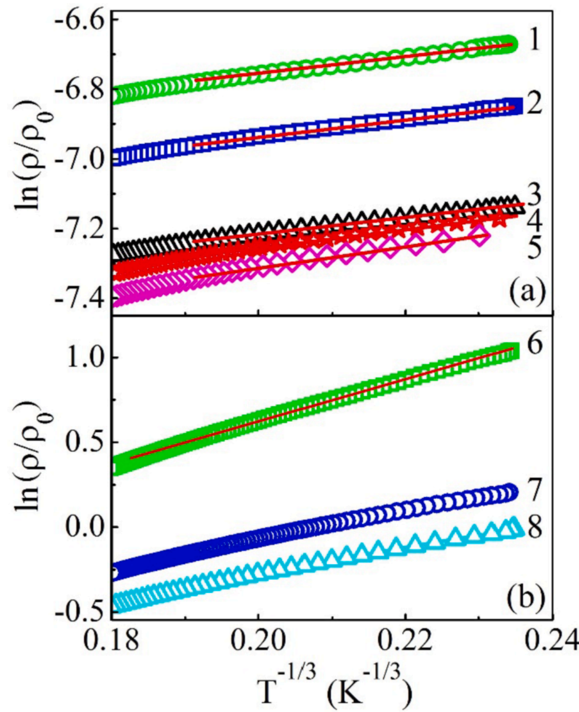

Fig. 10. Temperature dependence of resistivity in the $\ln\rho \sim 1/T^{1/3}$ coordinates for thin $(ZnO/C)_{81}$ (a) and $(ZnO/C)_{25}$ (b) films with various thickness: 1–35 nm, 2–45 nm, 3–70 nm, 4–98 nm, 5–129 nm, 6–150 nm, 7–157 nm, 8–169 nm.

Table 1
The *B*-parameter and density of states $g(E_F)$ at the Fermi level in eqs. (2) and (3) determined for $(ZnO–C)_{81}$ thin films.

h (nm)	$B(K^{1/3})$	$g(E_F)_{2D}$ ($eV^{-1}cm^{-2}$)
35	2.56	$3.2\cdot10^{17}$
45	2.52	$3.4\cdot10^{17}$
70	2.28	$4.6\cdot10^{17}$
98	2.75	$2.6\cdot10^{17}$
129	3.13	$1.8\cdot10^{17}$

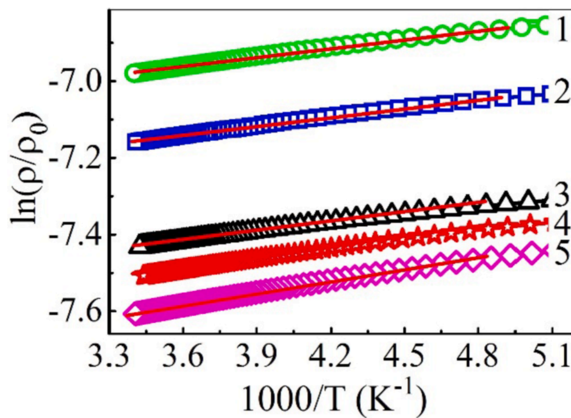

Fig. 11. Experimental (dots) and theoretically fitted (solid lines) using eq. (4) resistivity as a function of temperature for thin $(ZnO/C)_{81}$ films (1–35 nm, 2–45 nm, 3–70 nm, 4–98 nm, 5–129 nm).

Table 2
The hopping activation energy W_{NNH} (see eq. (4)) for thin $(ZnO/C)_{81}$ films in the temperature range of 200–300 K.

h (nm)	W_{NNH} (eV)
31	0.0068
45	0.0068
70	0.0066
98	0.0076
129	0.0089

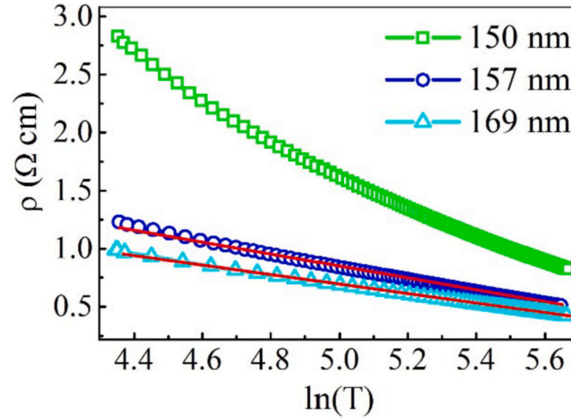

Fig. 12. Temperature dependence of resistivity for multilayer $(ZnO/C)_{25}$ heterostructures in the temperature range of 77–300 K in the ρ-ln(T) coordinates.

Fig. 9 shows the magnetization of the studied samples of various thicknesses as a function of the magnetic field. As seen in Fig. 9, ferromagnetism is not observed in the fabricated films at 10 K.

According to the literature [4,7,32], there are two scenarios for the formation of long-range magnetic ordering in ZnO-C films. In the first scenario, the carbon doping leads to a substitution of oxygen by carbon, with the formation of ZnC complexes, and generating the hole conductivity. This process initiates the ferromagnetic exchange between ZnC with the magnetic moment of 2.02 μB per C atom and affects the Curie temperature, exceeding 400 K. This scenario, was observed in Ref. [4] for the films fabricated by the pulsed laser deposition method. However, we rule out this first scenario, because our Hall and thermopower measurements demonstrate that the carbon doping does not produce the hole conductivity in the studied samples, which agrees with the work [8]. This scenario is not possible in our case because of the specific conditions of the layer-by-layer deposition method. It is worth noting, that according to the structural analysis, the ZnC phase was not detected. The second scenario is associated with the defect-induced magnetism(when the exchanging magnetic moments are formed on the dangling bonds [8]). Taking into account the electron concentration, contributing the conductivity, the presence of a large number of interfaces and the island structure produce a high defect concentration in our multilayer samples. However, we did not detect the ferromagnetism in the studied heterostructures. It does not rule out the possible formation of the magnetic moments on defects, but it seems that the exchange interaction is weak, making it lower the measurement equipment sensitivity.

The negative MR is usually considered as a consequence of the ferromagnetic ordering, but in our samples, there is no long-range magnetic order and it is necessary to conduct some extra investigations of samples with higher thickness. It is possible to explain the negative MR through quantum interference and non-interference mechanisms. The interference mechanisms are possible both in the case of variable-range hopping conductivity [33,34] and in the weak localization case (see, for example [35]). The logarithmic temperature dependence of resistivity attributed to weak localization in 2D systems (see Fig. 12) confirms the interference nature of negative MC. The charge transport occurs along the interfaces between ZnO and C. It is important to emphasize, that for the $(ZnO–C)_{81}$ films (h = 137 nm), having not continuous ZnO and C layers and demonstrating the hopping conductivity, resistivity does not depend on the magnetic field in the studied range. A specific noninterference mechanism, related to the non-spherical wave functions of electrons in the quantum wells, was proposed in Ref. [33]. This mechanism is characterized by a large value of MR (estimated to be MR = 15% [36]), a weak temperature dependence, and a linear dependence on the magnetic field. Since the field dependence is nonlinear at the temperature of 77 K, it is unlikely if the mentioned above mechanism takes place in our case. Besides, the formation of any well-defined quantum wells in the multilayer system $(ZnO/C)_{25}$ is highly doubtful. It is worth noting that in the $(ZnO/C)_{81}$ system, where the formation of quantum wells is potentially possible due to the island structure, a negative MR was found neither at room temperature nor at 77 K. Another non-interference mechanism is originated from the partial suppression of electron scattering on the magnetic moments of defects by an external magnetic field. This effect is similar to the magnetoresistance in the spin glasses or the

paramagnetic ferromagnetic alloys. In our samples, this mechanism is supported by the fact that MR takes place at room temperature. Besides, the observed field dependence of the negative MR is similar to the field dependence of squared magnetization at low and room temperature. However, based on this mechanism, the value of MR at room temperature has to be more than one order of magnitude less than that at 77 K, which is not observed in our samples. Also, the relatively large magnitude of MR makes this mechanism to be scarcely realized. Thus, the observed negative magnetoresistance in the multilayer $(ZnO/C)_{25}$ system can be attributed to weak localization and 2D charge transport along the interfaces between ZnO and C layers. More detailed further studies can clarify the possible mechanisms associated with this effect.

4. Conclusions

The thin $(ZnO/C)_{81}$ and $(ZnO/C)_{25}$ films were fabricated through the layer-by-layer deposition of ZnO and C by the ion-beam sputtering method at various deposition rates. The results of XRD analysis revealed that the $(ZnO/C)_{81}$ samples are not multilayers, rather the zinc oxide nanocrystallites are randomly embedded in an amorphous carbon matrix. Thin $(ZnO/C)_{25}$ films are multilayered, consisting of ZnO crystalline and amorphous C layers. It was revealed that $(ZnO/C)_{81}$ and $(ZnO/C)_{25}$ thin-film samples manifest the n-type conductivity, with the electrical resistivity of 1–2 orders of magnitude lower than that in ZnO films without C.

The conduction mechanism changes from the variable-range hopping in a narrow energy band near the Fermi level to the hopping to the nearest neighbor mechanism in thin $(ZnO/C)_{81}$ films with an island structure. The transition from an island to a continuous structure of ZnO layers with the multilayer thickness of about 150 nm is accompanied by the transition from the strong to weak localization of charge carriers, along with the conduction mechanism changes in the studied temperature range. The fabricated films do not exhibit ferromagnetism at the temperature range from 10 K to room temperature. In the multilayer $(ZnO/C)_{25}$ thin-film structures with various bilayer thicknesses the negative magnetoresistive effect was detected at $T = 77$ K and at $T = 300$ K. The magnitude and temperature dependence of MR cannot be explained in the framework of interference and non-interference mechanisms of negative magnetoresistance. The magnitude and temperature dependence of MR can be explained by weak localization and 2D charge transport along the interfaces between ZnO and C layers.

Declaration of competing interest

No conflict of interest exists.

Acknowledgments

The work was supported by the Ministry of Education and Science of Russia (project No. 3.1867.2017/4.6) and the RFBR (project No. 19-07-00471). The work was partially funded by the Academy of Finland.

References

[1] T. Dietl, A ten-year perspective on dilute magnetic semiconductors and oxides, Nat. Mater. 9 (2010) 965–974, https://doi.org/10.1038/nmat2898.
[2] O. Volnianska, P. Boguslawski, Magnetism of solids resulting from spin polarization of p orbitals, J. Phys. Condens. Matter 22 (2010), https://doi.org/10.1088/0953-8984/22/7/073202.
[3] M. Venkatesan, C.B. Fitzgerald, J.M.D. Coey, Unexpected magnetism in a dielectric oxide, Nature 430 (2004) 630, https://doi.org/10.1038/430630a.
[4] H. Pan, J.B. Yi, L. Shen, R.Q. Wu, J.H. Yang, J.Y. Lin, Y.P. Feng, J. Ding, L.H. Van, J.H. Yin, Room-temperature ferromagnetism in carbon-doped ZnO, Phys. Rev. Lett. 99 (2007) 127201, https://doi.org/10.1103/PhysRevLett.99.127201.
[5] X.J. Ye, H.A. Song, W. Zhong, M.H. Xu, X.S. Qi, C.Q. Jin, Z.X. Yang, C.T. Au, Y.W. Du, The effect of nitrogen incorporation on the magnetic properties of carbon-doped ZnO, J. Phys. D Appl. Phys. 41 (2008), https://doi.org/10.1088/0022-3727/41/15/155005.
[6] K. Tang, S. Gu, S. Zhu, W. Liu, J. Ye, J. Zhu, R. Zhang, Y. Zheng, X. Sun, Carbon clusters in N-doped ZnO by metal-organic chemical vapor deposition, Appl. Phys. Lett. 93 (2008), https://doi.org/10.1063/1.2992197.
[7] X. Wang, X. Chen, R. Dong, Y. Huang, W. Lu, Ferromagnetism in carbon-doped ZnO films from first-principle study, Phys. Lett. Sect. A Gen. At. Solid State Phys. 373 (2009) 3091–3096, https://doi.org/10.1016/j.physleta.2009.06.049.
[8] S.-H. Choi, D. Lim, J.W. Park, D.H. Kim, M. Lee, The role of carbon doping in ZnO, J. Kor. Phys. Soc. 57 (2010) 1482–1485, https://doi.org/10.3938/jkps.57.1482.
[9] M. Venkatesan, C.B. Fitzgerald, J.M.D. Coey, Unexpected magnetism in a dielectric oxide, Nature 430 (2004) 630, https://doi.org/10.1038/430630a.
[10] N.H. Hong, N. Poirot, J. Sakai, Ferromagnetism observed in pristine Sn O2 thin films, Phys. Rev. B Condens. Matter 77 (2008), https://doi.org/10.1103/PhysRevB.77.033205.
[11] G.Z. Xing, J.B. Yi, D.D. Wang, L. Liao, T. Yu, Z.X. Shen, C.H.A. Huan, T.C. Sum, J. Ding, T. Wu, Strong correlation between ferromagnetism and oxygen deficiency in Cr-doped In2 O3-δ nanostructures, Phys. Rev. B Condens. Matter 79 (2009), https://doi.org/10.1103/PhysRevB.79.174406.
[12] C.M. Araujo, M. Kapilashrami, X. Jun, O.D. Jayakumar, S. Nagar, Y. Wu, C. Århammar, B. Johansson, L. Belova, R. Ahuja, G.A. Gehring, K.V. Rao, Room temperature ferromagnetism in pristine MgO thin films, Appl. Phys. Lett. 96 (2010), https://doi.org/10.1063/1.3447376.
[13] L. Liao, B. Yan, Y.F. Hao, G.Z. Xing, J.P. Liu, B.C. Zhao, Z.X. Shen, T. Wu, L. Wang, J.T.L. Thong, C.M. Li, W. Huang, T. Yu, P -type electrical, photoconductive, and anomalous ferromagnetic properties of Cu2 O nanowires, Appl. Phys. Lett. 94 (2009), https://doi.org/10.1063/1.3097029.
[14] H. Peng, H.J. Xiang, S.H. Wei, S.S. Li, J.B. Xia, J. Li, Origin and enhancement of hole-induced ferromagnetism in first-row d0 semiconductors, Phys. Rev. Lett. 102 (2009), https://doi.org/10.1103/PhysRevLett.102.017201.
[15] H.K. Chandra, P. Mahadevan, Defect induced local moment in ZnO as a consequence of Stoner mechanism, Solid State Commun. 152 (2012) 762–766, https://doi.org/10.1016/j.ssc.2012.01.050.
[16] E. Stoner, Collective electron ferronmagnetism, Proc. R. Soc. London. Ser. A. Math. Phys. Sci. 165 (1938) 372–414, https://doi.org/10.1098/rspa.1938.0066.
[17] T.L. Phan, Y.D. Zhang, D.S. Yang, N.X. Nghia, T.D. Thanh, S.C. Yu, Defect-induced ferromagnetism in ZnO nanoparticles prepared by mechanical milling, Appl. Phys. Lett. 102 (2013), https://doi.org/10.1063/1.4793428.
[18] C.S. Ong, T.S. Herng, X.L. Huang, Y.P. Feng, J. Ding, Strain-induced ZnO spinterfaces, J. Phys. Chem. C 116 (2012) 610–617, https://doi.org/10.1021/jp205251z.

[19] D. Wang, Z.Q. Chen, D.D. Wang, N. Qi, J. Gong, C.Y. Cao, Z. Tang, Positron annihilation study of the interfacial defects in ZnO nanocrystals: correlation with ferromagnetism, J. Appl. Phys. 107 (2010), https://doi.org/10.1063/1.3291134.
[20] V.A. Coleman, C. Jagadish, Basic properties and applications of ZnO, in: Zinc Oxide Bulk, Thin Film, Nanostructures, Elsevier Ltd, 2006, pp. 1–20, https://doi.org/10.1016/B978-008044722-3/50001-4.
[21] V.V. Rylkov, S.N. Nikolaev, V.A. Demin, A.V. Emelyanov, A.V. Sitnikov, K.E. Nikiruy, V.A. Levanov, M.Y. Presnyakov, A.N. Taldenkov, A.L. Vasiliev, K. Y. Chernoglazov, A.S. Vedeneev, Y.E. Kalinin, A.B. Granovsky, V.V. Tugushev, A.S. Bugaev, Transport, magnetic, and memristive properties of a nanogranular (CoFeB) x (LiNbO y)100–x composite material, J. Exp. Theor. Phys. 126 (2018) 353–367, https://doi.org/10.1134/S1063776118020152.
[22] Y.E. Kalinin, M.A. Kashirin, V.A. Makagonov, S.Y. Pankov, A.V. Sitnikov, Properties of amorphous carbon thin films grown by ion beam sputtering, Tech. Phys. 62 (2017) 1724–1730, https://doi.org/10.1134/S1063784217110123.
[23] O.V. Zhilova, S.Y. Pankov, A.V. Sitnikov, Y.E. Kalinin, I.V. Babkina, The structure and the gas sensitive properties of the thin films of zinc oxide, in: AIP Conf. Proc., AIP Publishing LLC, 2017, 020054, https://doi.org/10.1063/1.5002951.
[24] N.A. Lashkova, A.I. Maximov, A.A. Ryabko, A.A. Bobkov, V.A. Moshnikov, E.I. Terukov, Synthesis of ZnO-based nanostructures for heterostructure photovoltaic cells, Semiconductors 50 (2016) 1254–1260, https://doi.org/10.1134/S106378261609013X.
[25] T.A. Polyanskaya, Y.V. Shmartsev, Quantum corrections to the conductivity OF semiconductors with a two-dimensional and a 3-DIMENSIONAL electron-gas-experiments, Sov. Phys. Semiconduct. 23 (1989) 1–19.
[26] M. Nistor, F. Gherendi, J. Perrière, Degenerate and non-degenerate In2O3 thin films by pulsed electron beam deposition, Mater. Sci. Semicond. Process. 88 (2018) 45–50, https://doi.org/10.1016/J.MSSP.2018.07.024.
[27] O. V Zhilova, S.Y. Pankov, A.V. Sitnikov, Y.E. Kalinin, M.N. Volochaev, V.A. Makagonov, Structure and electrophysical properties of thin-film SnO2-In2O3 heterostructures, J. Mater. Sci. Electron. 30 (2019) 11859–11867.
[28] E.A.D.N.F. Mott, Electronic Processes in Non-crystalline Materials, Clarendon-Press, Oxford, 1971, https://doi.org/10.1002/crat.19720070420.
[29] G.V. Samsonov (Ed.), Handbook of the Physicochemical Properties of the Elements, Springer US, Boston, MA, 1968, https://doi.org/10.1007/978-1-4684-6066-7.
[30] Y. Li, Q. Huang, X. Bi, The change of electrical transport characterizations in Ga doped ZnO films with various thicknesses, J. Appl. Phys. 113 (2013), 053702, https://doi.org/10.1063/1.4789985.
[31] V. Bhosle, A. Tiwari, J. Narayan, Electrical properties of transparent and conducting Ga doped ZnO, J. Appl. Phys. 100 (2006), 033713, https://doi.org/10.1063/1.2218466.
[32] D.K. Mishra, J. Mohapatra, M.K. Sharma, R. Chattarjee, S.K. Singh, S. Varma, S.N. Behera, S.K. Nayak, P. Entel, Carbon doped ZnO: synthesis, characterization and interpretation, J. Magn. Magn Mater. 329 (2013) 146–152, https://doi.org/10.1016/J.JMMM.2012.09.058.
[33] B.L. Altshuler, A.G. Aronov, D.E. Khmelnitskii, Negative magnetoresistance in semiconductors in the hopping conduction region, JETP Lett. (Engl. Transl.) 36 (1982) 195–198.
[34] V.L. Nguyen, B.Z. Spivak, B.I. Shklovskii, Tunnel hopping in disordered systems, Sov. Phys. JETP 62 (1985) 1021–1029.
[35] T. Ohyama, M. Okamoto, E. Otsuka, Weak localization and correlation effects of two dimensional electrons in indium-tin-oxide films, J. Phys. Soc. Japan. 52 (1983) 3571–3578, https://doi.org/10.1143/JPSJ.52.3571.
[36] A.V. Shumilin, Negative magnetoresistance in the regime of hopping conduction through p states at quantum dots, JETP Lett. (Engl. Transl.) 95 (2012) 416–419, https://doi.org/10.1134/S0021364012080115.